Research article

# Involvement of pore helix in voltage-dependent inactivation of TRPM5 channel

Kunitoshi Uchida [a,b,*,1], Tomo Kita [a,c,1], Mitsutoki Hatta [a], Satoru G. Itoh [d,e], Hisashi Okumura [d,e], Makoto Tominaga [f,g], Jun Yamazaki [a,h]

[a] Department of Physiological Science and Molecular Biology, Fukuoka Dental College, Fukuoka, Fukuoka, 814-0193, Japan
[b] Department of Environmental and Life Sciences, School of Food and Nutritional Sciences, University of Shizuoka, Shizuoka, Shizuoka, 422-8526, Japan
[c] Department of Pharmacology, Faculty of Medicine, Fukuoka University, Fukuoka, Fukuoka, 814-0180, Japan
[d] Department of Theoretical and Computational Molecular Science, Institute for Molecular Science, Okazaki, Aichi, 444-8787, Japan
[e] Biomolecular Dynamics Simulation Group, The Exploratory Research Center on Life and Living Systems, Okazaki, Aichi, 444-8787, Japan
[f] Division of Cell Signaling, National Institute for Physiological Sciences, Okazaki, Aichi, 444-8787, Japan
[g] Thermal Biology Group, The Exploratory Research Center on Life and Living Systems, Okazaki, Aichi, 444-8787, Japan
[h] Laboratory of Veterinary Pharmacology, Department of Veterinary Medicine, Nihon University College of Bioresource Sciences, Fujisawa, Kanagawa, 252-0880, Japan

## ARTICLE INFO

## ABSTRACT

The transient receptor potential melastatin 5 (TRPM5) channel is a monovalent-permeable cation channel that is activated by intracellular $Ca^{2+}$. Expression of TRPM5 has been shown in taste cells, pancreas, brainstem and olfactory epithelium, and this channel is thought to be involved in controlling membrane potentials. In whole-cell patch-clamp recordings, TRPM5 exhibited voltage-dependent inactivation at negative membrane potentials and time constant of voltage-dependent inactivation of TRPM5 did not depend on the intracellular $Ca^{2+}$ concentrations between 100 and 500 nM. Alanine substitution at Y913 and I916 in the pore helix of TRPM5 increased time constant of voltage-dependent inactivation. Meanwhile, voltage-dependent inactivation was reduced in TRPM5 mutants having glycine substitution at L901, Y913, Q915 and I916 in the pore helix. From these results, we conclude that the pore helix in the outer pore loop might play a role in voltage-dependent inactivation of TRPM5.

## 1. Introduction

Transient receptor potential melastatin 5 (TRPM5) is a cation channel that is permeable to monovalent cations, but not divalent cations. Although most TRP channels have multiple ligands, there are few reports concerning TRPM5 ligands. Only one definitive activator for TRPM5 is intracellular $Ca^{2+}$, and increases in temperature or steviol glycosides potentiate its activation by intracellular $Ca^{2+}$ [1,2]. Meanwhile, extracellular acidification, zinc ion, and triphenylphosphine oxide inhibit TRPM5 activation [3–5]. Expression of TRPM5 channels is restricted to taste cells, the pancreas, the brainstem, olfactory epithelium and olfactory nerve, where they are involved in controlling membrane potentials [6]. Some reports indicated that TRPM5 has physiological functions associated with insulin secretion [7] and signaling of sweet tastes [8]. These functions are thought to result from $Na^+$ influx and membrane depolarization through TRPM5 activation by increases in intracellular

$Ca^{2+}$ concentrations ($[Ca^{2+}]_i$). An understanding of the voltage-dependency of TRPM5 channels could be important for defining the mechanisms by which TRPM5 modulate membrane potentials.

Like other TRP channels, TRPM5 is thought to have functions as a tetramer wherein each subunit has intracellular N- and C- termini separated by 6 transmembrane (TM) domains. The pore-forming loop lies between TM5 and TM6 [6,9]. This topology structure is supported by the cryo-EM structure analysis of TRPM4, which is also a $Ca^{2+}$-activated nonselective monovalent cation channel, and is highly homologous to TRPM5 [10,11]. Two molecular gates exist in TRP channels, an inner gate that formed by a bundle crossing the four TM6 transmembrane domains near the cytoplasmic side, and an outer gate that indicates a selective filter situated in the pore loop. The topology structure of TRP channels is similar to that of voltage-gated $K^+$ channels, which exhibit N- and C-type inactivation [12]. N-type inactivation occurs via a "ball and chain" mechanism that inhibits ion conduction through occlusion of the

---

* Corresponding author.
  E-mail address: kuchida@u-shizuoka-ken.ac.jp (K. Uchida).
[1] Equal contribution to this work.

inner pore by the N-terminal region. In contrast, C-type inactivation is thought to involve a subtle conformational change around the selectivity filter. TRP channels also exhibit voltage dependence and mutant analyses suggested that the pore helix is involved in voltage-dependent inactivation in TRPA1 and TRPP3 [13,14]. Although TRPM5-mediated currents also exhibit voltage dependence, its inactivation mechanisms remain unclear.

In this study, we demonstrate that voltage-dependent inactivation of TRPM5 is independent of $[Ca^{2+}]_i$ and that the pore helix in the outer pore loop could be involved in the voltage-dependent inactivation.

## 2. Results

First, we confirmed the voltage-dependency of TRPM5-mediated currents using a whole-cell patch-clamp method in HEK293T cells expressing mouse TRPM5 (mTRPM5). Application of step-pulses in the presence of 0 or 30 nM $Ca^{2+}$ did not evoke any current in HEK293T cells expressing mTRPM5. On the other hand, application of step-pulses in the presence of intracellular 100, 300 or 500 nM $Ca^{2+}$ produced currents that had a slowly-activated large outward components and a rapidly-declined inward components in HEK293T cells expressing mTRPM5, while currents in the presence of intracellular 100 nM $Ca^{2+}$ looked smaller than those seen in the presence of intracellular 300 and 500 nM $Ca^{2+}$ (Figure 1A). Furthermore, the kinetics of the activating current induced by 100 nM $Ca^{2+}$ at positive membrane potentials appeared to be slower than those by 300 and 500 nM $Ca^{2+}$, suggesting that this channel kinetics depend on $[Ca^{2+}]_i$ or its activity. The peak currents at -160 mV in the presence of 300 and 500 nM $Ca^{2+}$ were significantly larger than those in the presence of 0, 30 and 100 nM $Ca^{2+}$ (Figure 1B). We next analyzed the inactivation kinetics of mTRPM5 currents at -160 mV. The current ratio, which provides an indication of the inactivation ability, was similar among 100, 300 and 500 nM $Ca^{2+}$ (Figure 1C), although the peak current amplitude with 100 nM $Ca^{2+}$ was smaller than those in the presence of 300 nM and 500 nM $Ca^{2+}$. The inactivating time constants were not
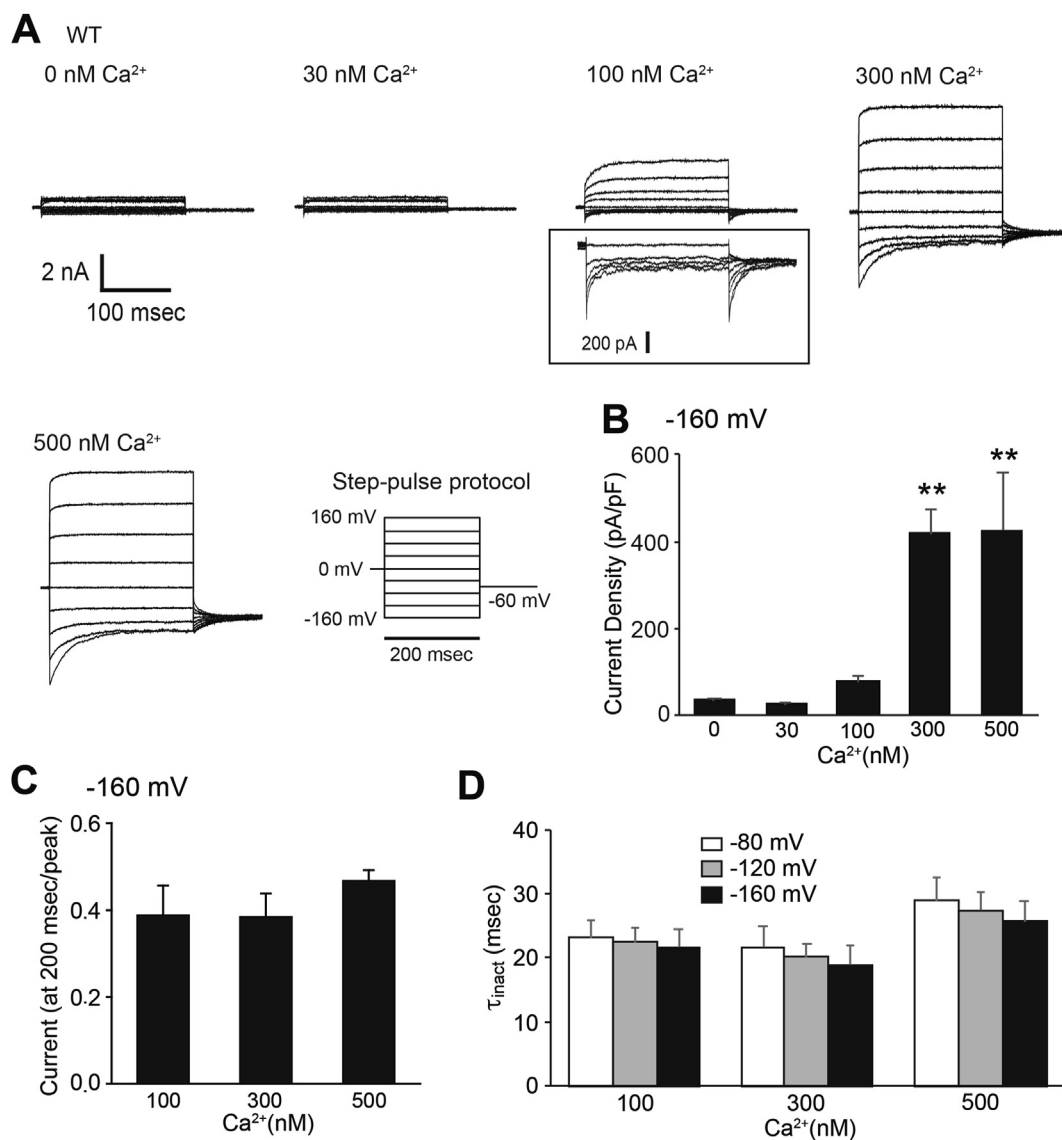


**Figure 1.** Relationship between intracellular $Ca^{2+}$ concentration and voltage dependency in the activation of TRPM5. (A) Representative traces of whole-cell currents stimulated by step-pulses in the presence of intracellular 0, 30, 100, 300 or 500 nM $Ca^{2+}$ in HEK293T cells expressing mouse TRPM5 (mTRPM5). Box indicates the current expanded from 100 nM $Ca^{2+}$-induced current at negative membrane potentials. The inset shows the step-pulse protocol. (B) Dose-response profiles of current densities in HEK293T cells expressing mTRPM5 activated by severl intracellular $Ca^{2+}$ concentrations at -160 mV. (C) The ratio of peak to steady-state (at 200 ms) current in HEK293T cells expressing mTRPM5 activated by 100, 300 or 500 nM $Ca^{2+}$ at -160 mV. (D) Inactivation time constant of whole-cell currents at -80, -120 or -160 mV in HEK293T cell expressing mTRPM5 activated by intracellular 100, 300 or 500 nM $Ca^{2+}$. Each column represents the mean + S.E.M. for 6–12 cells. Statistical significance was assessed using ANOVA followed by the two-tailed multiple t-test with Bonferroni correction. **; P < 0.01 vs. 0 or 30 nM $Ca^{2+}$.

largely different among at -80, -120 and -160 mV, suggesting that the inactivating time constants do not depend on membrane potentials (Figure 1D, and the representative fitting curves were shown in Figure 6A). Furthermore, the inactivating time constants were also not different among 100, 300 and 500 nM Ca$^{2+}$ (Figure 1D).

We hypothesized that the pore helix could be involved in the voltage-dependent inactivation of TRPM5. To test this hypothesis, we next constructed and analyzed mTRPM5 mutants. As shown in Figure 2A and B, 16 amino acids are thought to comprise the pore helix of TRPM5 channel based on alignment analysis of the amino acid sequence between TRPM4 and TRPM5. Therefore, we constructed single mutants in which alanine was substituted for each of the 16 amino acids in the pore helix (L901A, E902A, W903A, I904A, F905A, R906A, R907A, V908A, L909A, Y910A, R911A, P912A, Y913A, L914A, Q915A and I916A). We excluded W903A, R906A, R907A, L909A, Y910A, R911A, P912A and L914A mutants from analysis, because channels having these substitutions showed no current activation in response to step-pulses even in the presence of intracellular 500 nM Ca$^{2+}$ (Figure 3A). We confirmed the protein expression of TRPM5 mutants in HEK293T cells by immunocytochemistry using an anti-TRPM5 antibody. While TRPM5 L901A and L909A appeared to be localized to the intracellular organelles, fluorescent signals of TRPM5 wild-type (WT) and the other TRPM5 mutants was observed throughout the HEK293 cells (Figure 4), suggesting that the protein of TRPM5 mutants were expressed in HEK293 cells. We then examined the currents of L901A, E902A, I904A, F905A, V908A, Y913A, Q915A and I916A mutants in the presence of 500 nM Ca$^{2+}$, and found that inactivation of Y913A and I916A mutants at negative membrane potentials appeared to be weaker than that of TRPM5 WT (Figure 3A). Although the current ratios of TRPM5 mutants at -80, -120 and -160 mV did not differ from that for TRPM5 WT, the inactivation time constants ($\tau_{inact}$) at -120 and -160 mV for Y913A and I916A were significantly larger than that for TRPM5 WT (Figure 3B and C, and the representative fitting curves were shown in Figure 6B). On the other hand, the L901A, E902A, I904A, F905A, V908A and Q915A mutants exhibited inactivating kinetics that were similar to that of TRPM5 WT (Figure 3C).

We then constructed amino acid substitution with glycine, which has smallest side chain among the amino acids and destabilizes α-helix structures. As shown in Figure 5A, voltage-dependent inactivation at negative membrane potentials was impaired for the Y913G mutant, as well as for the Q915G mutant. Unfortunately, because the currents seen at negative membrane potentials were unable to be fitted by a single exponential curve and we could not calculate $\tau_{inact}$ for the Y913G and

Q915G mutants, we analyzed the current ratio at -160 mV. The current ratios for L901G, Y913G and Q915G mutants at -160 mV were significantly larger than that for TRPM5 WT (Figure 5B). We then analyzed the $\tau_{inact}$ for TRPM5 mutants in which the current ratios did not exhibit the significant differences. While the $\tau_{inact}$ value for E902G, F905G, V908G at -160 mV were not significantly different from that for WT, the $\tau_{inact}$ value for I916G at -160 mV was significantly larger than that for WT (Figure 5C, and the representative fitting curves were shown in Figure 6C).

Voltage-dependent inactivation of TRPM5 was impaired upon substitution of glutamine at 901 or 915 for glycine but not for alanine (Figures 3 and 5). Alanine and glycine are known to exhibit different effects on stabilization of helical conformations. To confirm the effects of each on stabilization of helical conformations, we analyzed the conformational stability of the pore helix and the selective filter by molecular dynamics simulations. We confirmed that substitution of glutamine at 915 to glycine reduced the stability of the α-helix structure of the pore helix. In addition, substitution of glutamine at 915 to glycine reduced the probability of the α-helix structure at F917 and increased the probability of the α-helix structure at G918 and Q919 compared to TRPM5 WT, while substitution to alanine did not affect to the structure of the selective filter from F917 to Q919 (Figure 7).

## 3. Discussion

In this study, we showed that TRPM5 channels exhibited voltage-dependent inactivation at negative membrane potentials that was independent of [Ca$^{2+}$]$_i$ (Figure 1). In addition, substitution of amino acids within the pore helix of TRPM5 channel impaired the voltage-dependent inactivation.

The peak amplitude of activating currents of TRPM5 depends on [Ca$^{2+}$]$_i$ above 100 nM at both positive and negative membrane potentials, which is similar to the report by another study [15]. On the other hand, inactivation of TRPM5 was independent of [Ca$^{2+}$]$_i$ (Figure 1). Changes in [Ca$^{2+}$]$_i$ to higher than 40 μM induce not only activation but also desensitization of TRPM5 in the excised patch membrane [4]. The time constant of desensitization were between 0.6 and 4 s, which are much larger than that for voltage-dependent inactivation (i.e., several dozens of ms), suggesting that mechanisms for Ca$^{2+}$-dependent desensitization and voltage-dependent inactivation are different. There are two major mechanisms for voltage dependence of TRP channels: 1) voltage-dependent pore blockage by divalent cations and 2) intrinsic
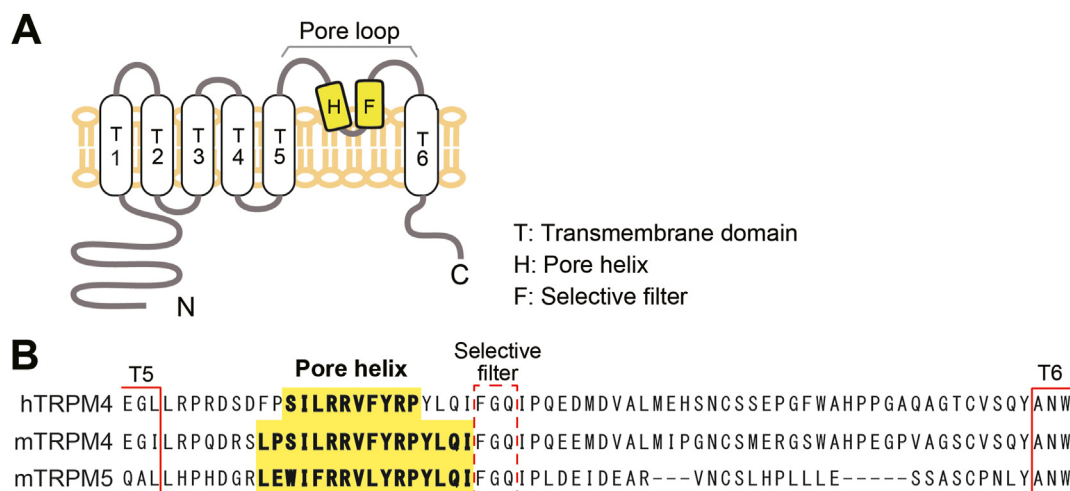


**Figure 2.** Putative amino acid sequence of the pore helix of mouse TRPM5. (A) Schematic diagram of mouse TRPM5 (mTRPM5). H: pore helix; F: selective filter; T: transmembrane domain. (B) Sequence alignment of the pore regions in human TRPM4 (hTRPM4), mTRPM4 and mTRPM5. Highlighted areas denote the pore helix region and areas outlined with a dotted line denote the selective filter. Structural information of hTRPM4 and mTRPM4 was referenced from cryo-EM structural analysis by Winkler et al. [11] and Guo et al. [10].
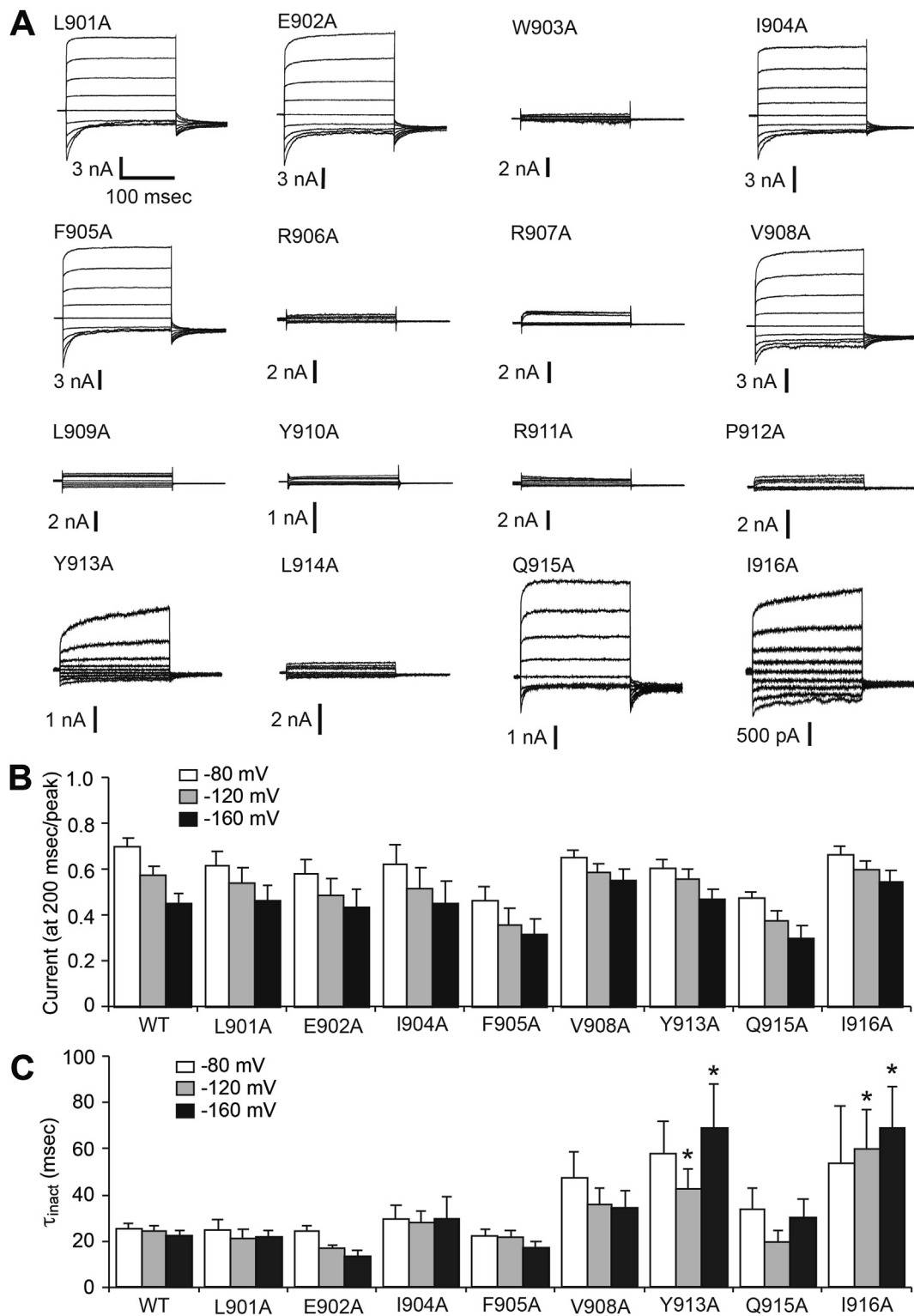
**Figure 3.** The effect of alanine substitutions in the pore helix region on voltage-dependent inactivation of mouse TRPM5. (A) Representative traces of whole-cell currents stimulated by step-pulses with intracellular 500 nM $Ca^{2+}$ in HEK293T cells expressing mTRPM5/L901A, E902A, W903A, I904A, F905A, R906A, R907A, V908A, L909A, Y910A, R911A, P912A, Y913A, L914A, Q915A and I916A mutants. (B) The ratio of peak to steady-state (at 200 ms) current in HEK293T cells expressing mTRPM5 wild-type (WT) and L901A, E902A, I904A, F905A, V908A, Y913A, Q915A or I916A mutants activated by 500 nM $Ca^{2+}$ at -80, -120 and -160 mV. (C) Inactivation time constant of whole-cell currents in HEK293T cells expressing mTRPM5 WT and L901A, E902A, I904A, F905A, V908A, Y913A, Q915A or I916A mutants activated by intracellular 500 nM $Ca^{2+}$ at -80, -120 and -160 mV. Each column represents the mean + S.E.M. for 6–18 cells. Statistical significance was assessed using Dunnett's test. *, P < 0.05 vs. WT.
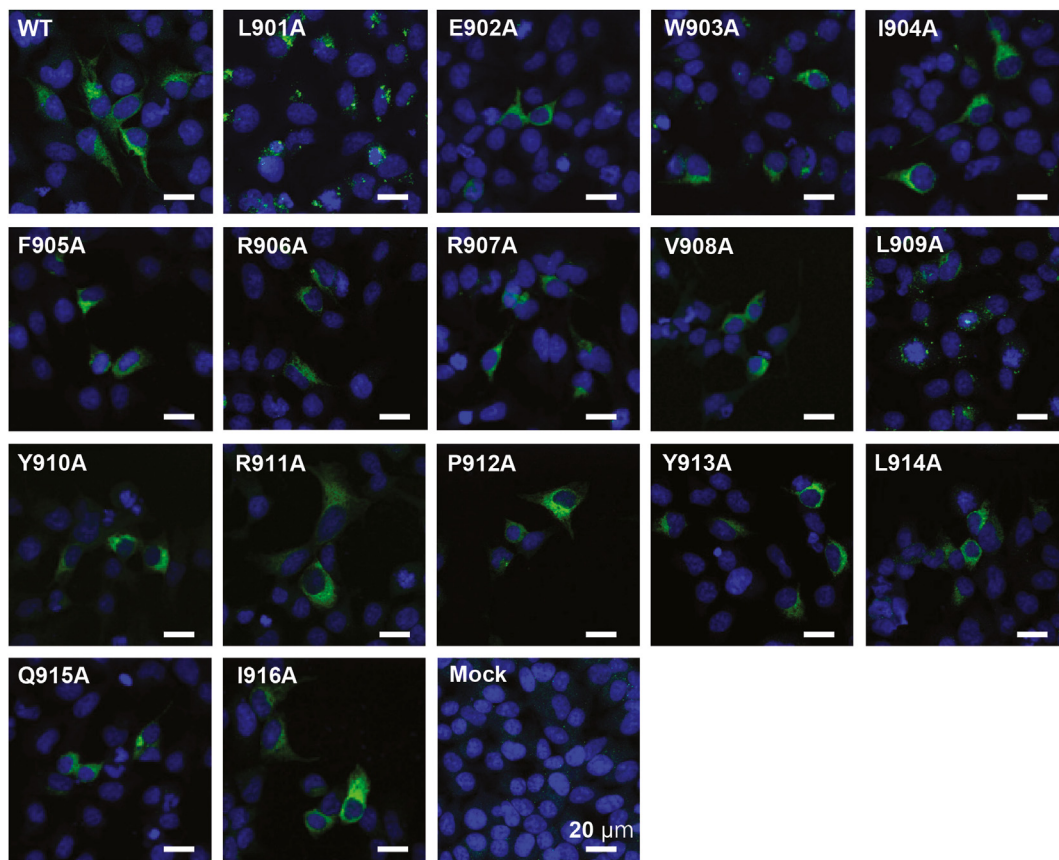
**Figure 4.** The expression of TRPM5 mutants in HEK293 cells. Immunocytochemistry of mouse TRPM5 wild-type (WT) and alanine-substituted mutants in HEK293 cells. Green indicates mouse TRPM5 WT or mutants and blue (pseudo-colour image) indicates the nuclei. Mock: mock-transfected HEK293 cells. Scale bar: 20 μm.

voltage-dependent gating [16]. Another possible mechanism is transition of the pore from an open state to an inactivated state that involves tilting of the lower portions of the TM6 helices toward the center of the pore, as is seen for the effect of calmodulin on TRPV6 [17]. TRPM4, which is closely related to TRPM5, also exhibits the voltage-dependent inactivation at negative membrane potentials, similar to that of TRPM5. Voltage dependence of TRPM4 does not appear to be affected by divalent cations [18]. In addition, voltage-dependent inactivation of TRPM4 can be observed in inside-out and outside-out configurations [18]. These reports and our findings may indicate that voltage-dependent inactivation of TRPM5 is not caused by the interaction with intracellular molecules such as $Ca^{2+}$ and calmodulin.

C-type inactivation is seen for voltage-gated $K^+$ channels, and structural analyses of the KcsA $K^+$ channel suggested that such inactivation results from a conformational change in the selective filter. X-ray crystal structure analysis of the KcsA channel [19] showed partial collapse of the selective filter prevents $K^+$ conduction. Functionally, mutation of glutamate at 71 in the pore helix, which is an adjacent subunit to the selectivity filter, abolished the inactivation ability of the KcsA channel [20]. Although glutamate, an amino acid with electrically charged side chain, is not conserved in voltage-gated $K^+$ channels, the structural rearrangement of hydrogen bond network between selective filter and pore helix rather than a protonation of E71 is reported to be important for the inactivation of KcsA channel [21]. C-type inactivation is conserved among voltage-gated $K^+$ channels, as studies with Shaker (KCNA3) channel demonstrated that substitution of amino acids within the pore helix impairs the inactivation [21]. In this study, we found that voltage-dependent inactivation of mTRPM5 at negative membrane potentials was impaired by substitution of amino acids within the pore helix (Figures 3 and 5), indicating that C-type inactivation could be involved in voltage-dependent inactivation of TRPM5 channels. It is also possible

that pore collapse underlie the voltage-dependent inactivation of TRPM5 channels. We and another group previously reported that zinc ion and proton inactivate TRPM5 irreversibly [3,22]. While TM5-TM6 region was involved in these irreversible inactivation, electrical interaction with charged amino acids (such as glutamate and aspartate) was necessary for its inactivation, suggesting that the different mechanisms underlie between voltage-dependent inactivation and irreversible inactivation by zinc ion and proton in TRPM5.

Interestingly, voltage-dependent inactivation of TRPM5 was impaired by substitution of glutamine at 915 to glycine but not to alanine (Figures 3 and 5) and substitution of glutamine at 915 to glycine can reduce the structural stability of the selective filter (Figure 7), suggesting that the pore helix structure could modulate the gating of selective filter for voltage-dependent inactivation. Voltage-dependent inactivation of TRPM5 was also impaired by substitution of leucine at 901 to glycine but not to alanine. Although we cannot make definitive conclusions, one possible explanation is that substitution of leucine at 901 to glycine affects the stability of the selective filter. We also found that Y913 and I916 are also involved in voltage-dependent inactivation (Figures 3 and 5). The side chains of Y971 and I974 in TRPM4, which correspond to Y913 and I916 in TRPM5, are at conformationally opposite sides of the selective filter and near TM5 and TM6 [10]. Although structural analysis of TRPM5 with atomic resolution, such as cryo-EM analysis, is necessary, it is possible that the Y913 and I916 could interact with TM5 and TM6, and that modulate voltage-dependent inactivation of TRPM5. Our results suggest that the latter part of the pore helix may play an important role in voltage-dependent inactivation. Further analysis will help elucidate the precise mechanisms of voltage-dependent inactivation of TRPM5.

Given that the amino acid sequences of the pore helix are highly conserved among TRPM channels (Figure 2B and [10]), similar mechanisms could also be associated with the voltage-dependent inactivation of
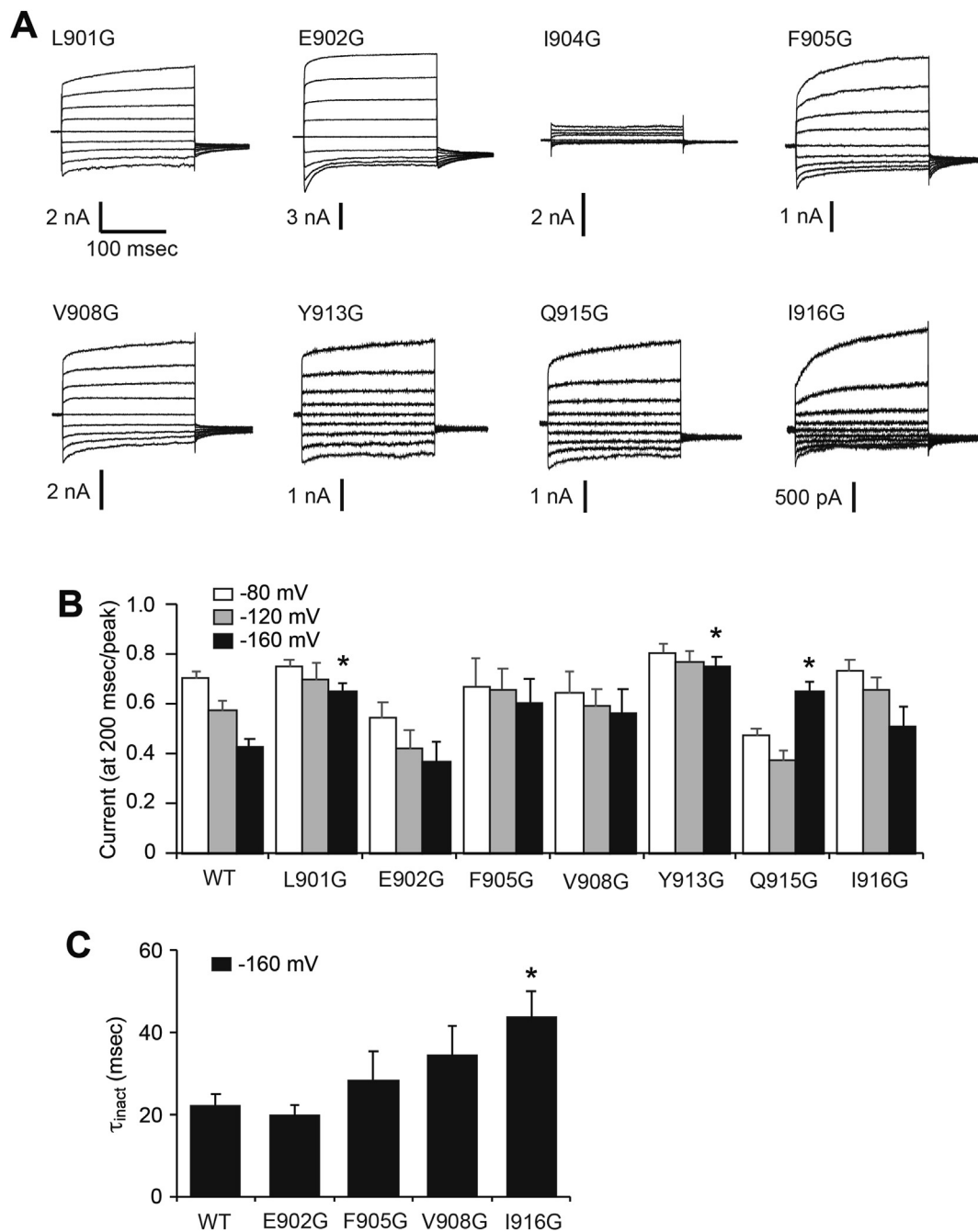
**Figure 5.** The effect of glycine substitution in the pore helix region on voltage-dependent inactivation of mouse TRPM5. (A) Representative traces of whole-cell currents stimulated by step-pulses with intracellular 500 nM $Ca^{2+}$ in HEK293T cells expressing mTRPM5 L901G, E902G, I904G, F905G, V908G, Y913G, Q915G and I916G mutants. (B) The ratio of peak to steady-state (at 200 ms) current in HEK293T cells expressing mTRPM5 WT and L901G, E902G, F905G, V908G, Y913G, Q915G or I916G mutants activated by 500 nM $Ca^{2+}$ at -80, -120 and -160 mV. (C) Inactivation time constant of whole-cell currents at -160 mV in HEK293T cells expressing mouse TRPM5 WT and E902G, F905G, V908G or I916G mutants activated by intracellular 500 nM $Ca^{2+}$ at -160 mV. Each column represents the mean + S.E.M. for 6–12 cells. Statistical significance was assessed using Dunnett's test. *, $P < 0.05$ vs. WT.

TRPM4. Comparison of the amino acid sequence of the pore regions of TRPM5 and TRPM4 demonstrate that the amino acid sequences of both the pore helix and the selective filter are highly conserved (Figure 2B), suggesting that the same mechanisms may underlie the voltage-dependent inactivation of TRPM4. Similar inactivation was also reported for other TRP channels, such as TRPM2 with same pore helix sequences, which exhibits inactivation by pore collapse caused by conformational changes in selective filter [23]. In TRPA1 channels, L906 in the pore helix is considered to be essential for voltage-dependent gating [13]. In case of TRPP3 (also named PKD2L1), N533 in the pore

loop region is essential for its voltage-dependent inactivation [24]. Thus, conformational dynamics of the pore region during voltage-dependent inactivation could be conserved among TRP channels.

## 4. Methods

### 4.1. Cell culture

Human embryonic kidney-derived 293T (HEK293T) cells were maintained in DMEM (WAKO Pure Chemical Industries, Ltd., Osaka,
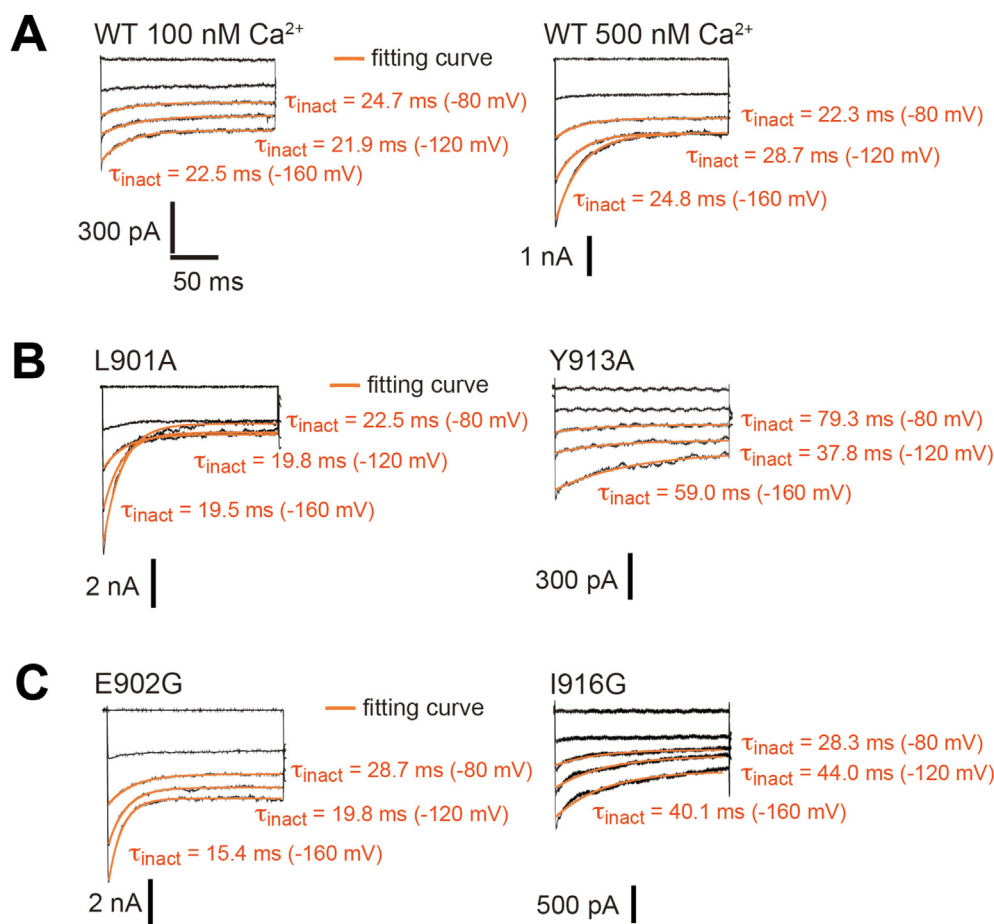
6

**Figure 6.** Representative fitting curve for determination of inactivation time constants. (A) Representative traces of whole-cell currents (black), fit with exponential functions (orange) stimulated by step-pulses in the presence of intracellular 100 or 500 nM $Ca^{2+}$ in HEK293T cells expressing mouse TRPM5 wild-type (WT). (B) Representative traces of whole-cell currents (black), fit with exponential functions (orange) stimulated by step-pulses in the presence of intracellular 500 nM $Ca^{2+}$ in HEK293T cells expressing mouse TRPM5 L901A and Y913A. (C) Representative traces of whole-cell currents (black), fit with exponential functions (orange) stimulated by step-pulses in the presence of intracellular 500 nM $Ca^{2+}$ in HEK293T cells expressing mouse TRPM5 E902G and I916G.
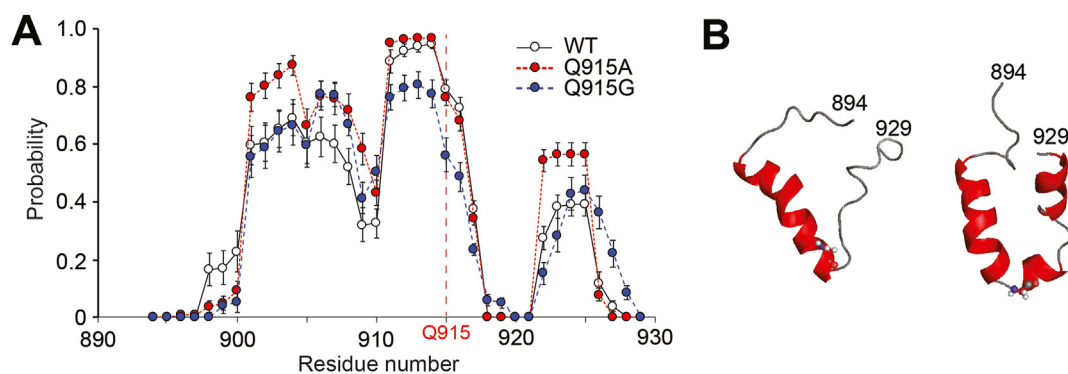


**Figure 7.** Results of molecular dynamics simulation confirming the stability of the structures of mouse TRPM5 wild-type, Q915A and Q915G. (A) Percent helical occupancy for each amino acid residue from L894 to R929 of mouse TRPM5 wild-type (WT), Q915A and Q915G. (B) Snapshots of the molecular dynamics simulation of mouse TRPM5 Q915G at 0 ns (left) and at 100 ns (right). Amino acid residues at 915 are shown in a stick representation.

Japan) containing 10% FBS (Thermo Fisher Scientific Inc, Massachusetts, USA), 100 units/mL penicillin (Thermo Fisher Scientific Inc), 100 μg/mL streptomycin (Thermo Fisher Scientific Inc), and 2 mM L-glutamine (GlutaMAX, Thermo Fisher Scientific Inc) at 37 °C in 5% $CO_2$. For patch-clamp recordings, 1 μg of plasmid DNA containing mouse TRPM5 in pcDNA3.1 and 0.1 μg pGreen Lantern 1 plasmid in OPTI-MEM medium (Thermo Fisher Scientific Inc) were transfected to HEK293T cells using Lipofectamine Plus Reagent (Thermo Fisher Scientific Inc). After incubating for 3–4 h, cells were reseeded on coverslips and further incubated at 37 °C in 5% $CO_2$. Whole-cell patch-clamp recordings were performed one day after transfection.

### 4.2. Construction of TRPM5 mutants

The mutants of mouse TRPM5 (mTRPM5) were made using a modified QuickChange Site-Directed Mutagenesis method (Stratagene Corp., California, USA), as we reported previously [25]. In detail, PCR was performed using mTRPM5 expression vectors as templates, two synthetic oligonucleotide primers containing specific mutations (Table 1), and PrimeSTAR Max DNA Polymerase (Takara Bio Inc., Shiga, Japan). The PCR products were digested with Dpn1 at 37 °C for 1 h and transformed into DH5α competent cells. The entire sequence including the desired substitution in the mutants was confirmed.

**Table 1.** Primers used for construction of TRPM5 mutants.

| Mutation | Sense Primer (5′→3′) | Antisense primer (5′→3′) |
| --- | --- | --- |
| L901A | CATGATGGCCGTGCGGAGTGGATTTTC | GAAAATCCACTCCGCACGGCCATCATG |
| E902A | GATGGCCGTTTGGCGTGGATTTTCCGC | GCGGAAAATCCACGCCAAACGGCCATC |
| W903A | GCCGTTTGGAGGCGATTTTCCGCCGT | ACGGCGGAAAATCGCCTCCAAACGGC |
| I904A | CGTTTGGAGTGGGCCTTCCGCCGTGTG | CACACGGCGGAAGGCCCACTCCAAACG |
| F905A | TTGGAGTGGATTGCCCGCCGTGTGCTA | TAGCACACGGCGGGCAATCCACTCCAA |
| R906A | GAGTGGATTTTCGCCCGTGTGCTATAC | GTATAGCACACGGGCGAAAATCCACTC |
| R907A | TGGATTTTCCGCGCTGTGCTATACAGG | CCTGTATAGCACAGCGCGGAAAATCCA |
| V908A | ATTTTCCGCCGTGCGCTATACAGGCCT | AGGCCTGTATAGCGCACGGCGGAAAAT |
| L909A | TTCCGCCGTGTGGCATACAGGCCTTAC | GTAAGGCCTGTATGCCACACGGCGGAA |
| Y910A | CGCCGTGTGCTAGCCAGGCCTTACCTG | CAGGTAAGGCCTGGCTAGCACACGGCG |
| R911A | CGTGTGCTATACGCGCCTTACCTGCAG | CTGCAGGTAAGGCGCGTATAGCACACG |
| P912A | GTGCTATACAGGGCTTACCTGCAGATC | GATCTGCAGGTAAGCCCTGTATAGCAC |
| Y913A | CTATACAGGCCTGCCCTGCAGATCTTT | AAAGATCTGCAGGGCAGGCCTGTATAG |
| L914A | TACAGGCCTTACGCGCAGATCTTTGG | CCAAAGATCTGCGCGTAAGGCCTGTA |
| Q915A | GGCCTTACCTGGCGATCTTTGGGC | GCCCAAAGATCGCCAGGTAAGGCC |
| I916A | CCTTACCTGCAGGCCTTTGGGCAAAT | ATTTGCCCAAAGGCCTGCAGGTAAGG |
| L901G | CATGATGGCCGTGGGGAGTGGATTTTC | GAAAATCCACTCCCCACGGCCATCATG |
| E902G | GATGGCCGTTTGGGGTGGATTTTCCGC | GCGGAAAATCCACCCCAAACGGCCATC |
| I904G | CGTTTGGAGTGGGGGTTCCGCCGTGTG | CACACGGCGGAAACCCCACTCCAAACG |
| F905G | TTGGAGTGGATTGGCCGCCGTGTGCTA | TAGCACACGGCGGCCAATCCACTCCAA |
| V908G | ATTTTCCGCCGTGGGCTATACAGGCCT | AGGCCTGTATAGCCCACGGCGGAAAAT |
| Y913G | ATACAGGCCTGGCCTGCAGATC | GATCTGCAGGCCAGGCCTGTAT |
| Q915G | CTTACCTGGGGATCTTTGGGCA | TGCCCAAAGATCCCCAGGTAAG |
| I916G | TACCTGCAGGGCTTTGGGCAAATC | GATTTGCCCAAAGCCCTGCAGGTA |

### 4.3. Electrophysiology

HEK293T cells on coverslips were mounted in an open chamber (Warner Instruments LLC, Connecticut, USA) and superfused with a bath solution containing 140 mM NaCl, 5 mM KCl, 2 mM CaCl$_2$, 2 mM MgCl$_2$, 10 mM glucose and 10 mM HEPES (pH 7.4 with NaOH). The pipette solution was adjusted to a Ca$^{2+}$ concentration of 0, 30, 100, 300 or 500 nM (calculated by CaBuf; http://www.kuleuven.be/fysio/trp/cabuf) and was used for all experiments. The pipette solution contained 120 mM K-Aspartate, 10 mM KCl, 1 mM MgCl$_2$, 5 mM EGTA, 10 mM HEPES (pH 7.4 with KOH), and CaCl$_2$ was added as follow: 0 mM CaCl$_2$ for 0 nM Ca$^{2+}$, 1.603 mM CaCl$_2$ for 30 nM Ca$^{2+}$, 3.032 mM CaCl$_2$ for 100 nM Ca$^{2+}$, 4.105 mM CaCl$_2$ for 300 nM Ca$^{2+}$, or 4.428 mM CaCl$_2$ for 500 nM Ca$^{2+}$. Data from whole-cell voltage-clamp recordings were sampled at 10 kHz and filtered at 5 kHz for analysis (Axopatch200B amplifier with pCLAMP10 software, Axon Instruments, California, USA). The membrane potential was clamped at 0 mV and voltage step-pulses from -160 to +160 mV (200 ms) were applied every second. All experiments were performed at room temperature (RT).

The inactivating time constant was estimated by fitting a single exponential curve between the peak current and the stimulus offset (200 ms):

$$I = A \times \exp(-t / \tau_{inact}) + I_o$$

Representative curve fittings were shown in Figure 6.
The current ratio was calculated as follow:
The current ratio = the current amplitude at 200 ms (steady-state)/ the peak current amplitude.
Analysis of currents was performed using pCLAMP10 software.

### 4.4. Immunocytochemistry

HEK293 cells were cultured on collagen I and poly-L-lysine-coated 4-well slides (Lab-Tek II chamber slide, Thermo Fisher Scientific Inc), and incubated with Lipofectamine 3000 reagent (Thermo Fisher Scientific

Inc) with 0.5 μg of each plasmid per well. Two days later, the cells were treated with 4% paraformaldehyde (15 min, 37 °C) and then 0.1% TritonX-100 (5 min, RT), followed by incubation with 10% goat serum. Then, the cells were incubated with anti-TRPM5 (1:200, Cat No. 18027-1-AP, Proteintech, Illinois, USA) for 2 h at RT, followed by a 1-hour incubation with anti-rabbit IgG-Alexa Fluor 488 (1:800, Abcam, Cambridge, UK) and TO-PRO-3 iodide (1:800, Thermo Fisher Scientific Inc) at RT. Fluorescence was observed using a confocal microscope (LSM510; Carl Zeiss MicroImaging GmbH, Jena, Germany). ZEN 2009 (Carl Zeiss) was used for image processing.

### 4.5. Molecular dynamics simulations

Molecular dynamics (MD) simulations were carried out to investigate the structures of the pore helix regions of TRPM5, Q915A and Q915G. Residues 894–929 were employed as the pore helix region in our MD simulations. Because the tertiary structure of TRPM5 has not yet been determined, the tertiary structure of TRPM4 (PDB ID: 6BCL) was utilized for modeling the pore helix regions of TRPM5 and its mutants. We obtained the initial structures by replacing the sidechains in TRPM4 with those in TRPM5 (or the mutants). The N- and C- termini were capped by ace- and N-methyl group, respectively. Each system consisted of one chain of the respective pore helix regions, one sodium ion, and water molecules. The number of water molecules was 3015 for the WT and Q915A systems and 3016 for the Q915G system. These molecules were prepared in a cubic simulation box with a side length of 46.608 Å. Four different initial velocities were prepared for the statistical analysis. MD simulations were performed by the Generalized-Ensemble Molecular Biophysics (GEMB) program [26], which was developed by one of the authors (H. Okumura). This program has been applied for several protein and peptide systems [27,28]. We applied the AMBER parm14SB force field [29] for the peptides and counter ions, and the TIP3P rigid body model [30] for the water by adopting the symplectic [31] quaternion scheme [32,33]. The electrostatic potential was calculated using the particle mesh Ewald (PME) method [34]. The cut-off distance was 12 Å for the Lennard-Jones (LJ) potential. To maintain the N- and C- terminal

positions, $C_\alpha$ atoms of the 894L and 929R residues were restrained with a harmonic potential, as in ref [27]. Reversible multiple time-step MD techniques were also applied. The time step was taken to be $\Delta t = 0.5$ fs for the bonding interactions of the peptide atoms, $\Delta t = 2.0$ fs for the Lennard-Jones (LJ) interactions and the real part of the PME calculation of the peptide atoms, and those between the peptide atoms and solvent molecules, and $\Delta t = 4.0$ fs for the LJ interaction and the real part of PME calculation between the solvent molecules and the reciprocal part of the PME calculation of all atoms. Because the symplectic rigid body algorithm was used for the water molecules, $\Delta t$ can be taken to be as long as 4.0 fs [33]. MD simulations in the canonical ensemble were performed for 100 ns at 310 K. The temperature was controlled using the Nosé–Hoover thermostat [35,36,37]. The first 20 ns simulation was regarded as the equilibration, and the following 80 ns simulation was used for the analysis. Error bars in physical quantities were calculated for the four MD simulations from the different initial conditions by the Bootstrap method with $10^6$ bootstrap cycles [38].

### 4.6. Statistical analysis

Data are expressed as means ± standard error of the mean (S.E.M.). Statistical analysis was performed by the unpaired two-tailed Student's $t$-test for comparison between two groups. Statistical analysis was performed by one-way analysis of variance (ANOVA) followed by a two-tailed multiple $t$-test with Bonferroni correction for comparison of multiple groups, or Dunnett's test for comparison with the control group using the Origin9 software (Origin Lab Corp., Massachusetts, USA). P values less than 0.05 were considered significant.

### Declarations

#### Author contribution statement

Kunitoshi Uchida: Conceived and designed the experiments; Performed the experiments; Analyzed and interpreted the data; Contributed reagents, materials, analysis tools or data; Wrote the paper.

Tomo Kita: Conceived and designed the experiments; Performed the experiments; Analyzed and interpreted the data.

Mitsutoki Hatta: Contributed reagents, materials, analysis tools or data.

Makoto Tominaga: Analyzed and interpreted the data; Contributed reagents, materials, analysis tools or data; Wrote the paper.

Jun Yamazaki, Satoru G. Itoh, Hisashi Okumura: Performed the experiments; Analyzed and interpreted the data; Contributed reagents, materials, analysis tools or data; Wrote the paper.

#### Data availability statement

Data included in article/supplementary material/referenced in article.

#### Declaration of interests statement

The authors declare no conflict of interest.

#### Additional information

No additional information is available for this paper.

### References

[1] K. Talavera, K. Yasumatsu, T. Voets, G. Droogmans, N. Shigemura, Y. Ninomiya, R.F. Margolskee, B. Nilius, Heat activation of TRPM5 underlies thermal sensitivity of sweet taste, Nature 438 (2005) 1022–1025, nature04248.

[2] K. Philippaert, A. Pironet, M. Mesuere, W. Sones, L. Vermeiren, S. Kerselaers, S. Pinto, A. Segal, N. Antoine, C. Gysemans, J. Laureys, K. Lemaire, P. Gilon, E. Cuypers, J. Tytgat, C. Mathieu, F. Schuit, P. Rorsman, K. Talavera, T. Voets, R. Vennekens, Steviol glycosides enhance pancreatic beta-cell function and taste sensation by potentiation of TRPM5 channel activity, Nat. Commun. 8 (2017) 14733.

[3] D. Liu, Z. Zhang, E.R. Liman, Extracellular acid block and acid-enhanced inactivation of the Ca2+-activated cation channel TRPM5 involve residues in the S3-S4 and S5-S6 extracellular domains, J. Biol. Chem. 280 (2005) 20691–20699. M414072200 [pii].

[4] D. Liu, E.R. Liman, Intracellular Ca2+ and the phospholipid PIP2 regulate the taste transduction ion channel TRPM5, Proc. Natl. Acad. Sci. U. S. A. 100 (2003) 15160–15165, 2334159100 [pii].

[5] D. Prawitt, M.K. Monteilh-Zoller, L. Brixel, C. Spangenberg, B. Zabel, A. Fleig, R. Penner, TRPM5 is a transient Ca2+-activated cation channel responding to rapid changes in [Ca2+]i, Proc. Natl. Acad. Sci. U. S. A. 100 (2003) 15166–15171, 2334624100 [pii].

[6] E.R. Liman, TRPM5 and taste transduction, in: B.N. Veit Flockerzi (Ed.), Handb Exp Pharmacol, Springer, 2007, pp. 287–298.

[7] B. Colsoul, A. Schraenen, K. Lemaire, R. Quintens, L. Van Lommel, A. Segal, G. Owsianik, K. Talavera, T. Voets, R.F. Margolskee, Z. Kokrashvili, P. Gilon, B. Nilius, F.C. Schuit, R. Vennekens, Loss of high-frequency glucose-induced Ca2+ oscillations in pancreatic islets correlates with impaired glucose tolerance in Trpm5-/- mice, Proc. Natl. Acad. Sci. U. S. A. 107 (2010) 5208–5213, 0913107107 [pii].

[8] C.A. Perez, L. Huang, M. Rong, J.A. Kozak, A.K. Preuss, H. Zhang, M. Max, R.F. Margolskee, A transient receptor potential channel expressed in taste receptor cells, Nat. Neurosci. 5 (2002) 1169–1176, nn952 [pii].

[9] T. Enklaar, M. Esswein, M. Oswald, K. Hilbert, A. Winterpacht, M. Higgins, B. Zabel, D. Prawitt, Mtr1, a novel biallelically expressed gene in the center of the mouse distal chromosome 7 imprinting cluster, is a member of the Trp gene family, Genomics 67 (2000) 179–187. S0888-7543(00)96234-7 [pii].

[10] J. Guo, J. She, W. Zeng, Q. Chen, X.C. Bai, Y. Jiang, Structures of the calcium-activated, non-selective cation channel TRPM4, Nature 552 (2017) 205–209.

[11] P.A. Winkler, Y. Huang, W. Sun, J. Du, W. Lu, Electron cryo-microscopy structure of a human TRPM4 channel, Nature 552 (2017) 200–204.

[12] H.T. Kurata, D. Fedida, A structural interpretation of voltage-gated potassium channel inactivation, Prog. Biophys. Mol. Biol. 92 (2006) 185–208.

[13] X. Wan, Y. Lu, X. Chen, J. Xiong, Y. Zhou, P. Li, B. Xia, M. Li, M.X. Zhu, Z. Gao, Bimodal voltage dependence of TRPA1: mutations of a key pore helix residue reveal strong intrinsic voltage-dependent inactivation, Pflügers Archiv 466 (2014) 1273–1287.

[14] T. Shimizu, A. Janssens, T. Voets, B. Nilius, Regulation of the murine TRPP3 channel by voltage, pH, and changes in cell volume, Pflügers Archiv 457 (2009) 795–807.

[15] T. Hofmann, V. Chubanov, T. Gudermann, C. Montell, TRPM5 is a voltage-modulated and Ca(2+)-activated monovalent selective cation channel, Curr. Biol. 13 (2003) 1153–1158. S0960982203004317 [pii].

[16] B. Nilius, K. Talavera, G. Owsianik, J. Prenen, G. Droogmans, T. Voets, Gating of TRP channels: a voltage connection? J. Physiol. 567 (2005) 35–44.

[17] A.K. Singh, L.L. McGoldrick, E.C. Twomey, A.I. Sobolevsky, Mechanism of calmodulin inactivation of the calcium-selective TRP channel TRPV6, Sci Adv 4 (2018), eaau6088.

[18] B. Nilius, J. Prenen, G. Droogmans, T. Voets, R. Vennekens, M. Freichel, U. Wissenbach, V. Flockerzi, Voltage dependence of the Ca2+-activated cation channel TRPM4, J. Biol. Chem. 278 (2003) 30813–30820.

[19] Y. Zhou, J.H. Morais-Cabral, A. Kaufman, R. MacKinnon, Chemistry of ion coordination and hydration revealed by a K+ channel-Fab complex at 2.0 A resolution, Nature 414 (2001) 43–48.

[20] J.F. Cordero-Morales, L.G. Cuello, Y. Zhao, V. Jogini, D.M. Cortes, B. Roux, E. Perozo, Molecular determinants of gating at the potassium-channel selectivity filter, Nat. Struct. Mol. Biol. 13 (2006) 311–318.

[21] D.M. Kim, C.M. Nimigean, Voltage-gated potassium channels: a structural examination of selectivity and gating, Cold Spring Harb Perspect Biol 8 (2016).

[22] K. Uchida, M. Tominaga, Extracellular zinc ion regulates transient receptor potential melastatin 5 (TRPM5) channel activation through its interaction with a pore loop domain, J. Biol. Chem. 288 (2013) 25950–25955.

[23] B. Toth, L. Csanady, Pore collapse underlies irreversible inactivation of TRPM2 cation channel currents, Proc. Natl. Acad. Sci. U. S. A. 109 (2012) 13440–13445.

[24] T. Shimizu, T. Higuchi, T. Toba, C. Ohno, T. Fujii, B. Nilius, H. Sakai, The asparagine 533 residue in the outer pore loop region of the mouse PKD2L1 channel is essential for its voltage-dependent inactivation, FEBS Open Bio 7 (2017) 1392–1401.

[25] T. Komatsu, K. Uchida, F. Fujita, Y. Zhou, M. Tominaga, Primary alcohols activate human TRPA1 channel in a carbon chain length-dependent manner, Pflügers Archiv 463 (2012) 549–559.

[26] H. Okumura, Temperature and pressure denaturation of chignolin: folding and unfolding simulation by multibaric-multithermal molecular dynamics method, Proteins 80 (2012) 2397–2416.

[27] R. Gupta, S. Saito, Y. Mori, S.G. Itoh, H. Okumura, M. Tominaga, Structural basis of TRPA1 inhibition by HC-030031 utilizing species-specific differences, Sci. Rep. 6 (2016) 37460.

[28] H. Okumura, S.G. Itoh, Transformation of a design peptide between the alpha-helix and beta-hairpin structures using a helix-strand replica-exchange molecular dynamics simulation, Phys. Chem. Chem. Phys. 15 (2013) 13852–13861.

[29] J.A. Maier, C. Martinez, K. Kasavajhala, L. Wickstrom, K.E. Hauser, C. Simmerling, ff14SB: improving the accuracy of protein side chain and backbone parameters from ff99SB, J. Chem. Theor. Comput. 11 (2015) 3696–3713.

[30] W.L. Jorgensen, J. Chandrasekhar, J.D. Madura, R.W. Impey, M.L. Klein, Comparison of simple potential functions for simulating liquid water, J. Chem. Phys. 79 (1983) 926–935.

[31] H. Yoshida, Construction of higher-order symplectic integrators, Phys. Lett. 150 (1990) 262–268.

[32] T.F. Miller, M. Eleftheriou, P. Pattnaik, A. Ndirango, D. Newns, G.J. Martyna, Symplectic quaternion scheme for biophysical molecular dynamics, J. Chem. Phys. 116 (2002) 8649–8659.

[33] H. Okumura, S.G. Itoh, Y. Okamoto, Explicit symplectic integrators of molecular dynamics algorithms for rigid-body molecules in the canonical, isobaric-isothermal, and related ensembles, J. Chem. Phys. 126 (2007). Artn 084103.

[34] U. Essmann, L. Perera, M.L. Berkowitz, T. Darden, H. Lee, L.G. Pedersen, A smooth particle mesh Ewald method, J. Chem. Phys. 103 (1995) 8577–8593.

[35] S. Nosé, A molecular-dynamics method for simulations in the canonical ensemble, Mol. Phys. 52 (1984) 255–268.

[36] S. Nosé, A unified formulation of the constant temperature molecular-dynamics methods, J. Chem. Phys. 81 (1984) 511–519.

[37] W.G. Hoover, Canonical dynamics - equilibrium phase-space distributions, Phys. Rev. 31 (1985) 1695–1697.

[38] B. Efron, 1977 rietz lecture - bootstrap methods - another look at the Jackknife, Ann. Stat. 7 (1979) 1–26.